Available online at www.sciencedirect.com
SCIENCE DIRECT®
ELSEVIER
International Journal of Multiphase Flow 29 (2003) 1645–1667
International Journal of Multiphase Flow
www.elsevier.com/locate/ijmulflow

Fluctuations of particle concentration in a turbulent two-phase shear layer

Y. Hardalupas [a,*], S. Horender [b]

[a] Department of Mechanical Engineering, Imperial College London, Exhibition Road, London SW7 2BX, UK
[b] DLR, Bunsenstr. 10, Göttingen 37073, Germany

Received 26 September 2002; received in revised form 29 July 2003

Abstract

Measurements and calculations of mean and rms of fluctuations of particle velocities and concentration and cross-correlation coefficients of two particle velocity components and concentration fluctuations in a horizontal plane shear layer laden with glass beads with mean diameters 55 and 90 μm are presented. The particles were injected at the low speed side of the flow, which is different from previous studies, and enhances the influence of gravity on particle dispersion. The ranges of Stokes numbers, based on the time scale of the large eddies, were 0.2–0.6 and 0.6–1.4 for 55 and 90 μm respectively. The particle gravitational settling parameter, due to gravity acting normal to the main flow direction at the low speed side of the shear layer, was for the mean flow 0.2 and 0.5 and for the turbulent flow 0.5 and 1 for 55 and 90 μm respectively. Velocity measurements were obtained by particle image velocimetry (PIV) and instantaneous particle concentration by counting the number of particles in each interrogation cell of the PIV images. The effect of interrogation cell size on instantaneous particle concentration was assessed and an appropriate interrogation cell size was chosen to quantify the non-random contribution of particle concentration fluctuations. The intensity of spatially-resolved non-random concentration fluctuations varied between 0.6 and 0.9 of the local mean concentration at the edge of the shear layer, where particles dispersed only due to centrifuging by fluid flow large scale structures and between 0.15 and 0.35 in the central region of the shear layer, where particles are convected by the flow or arrive due to centrifuging from the fluid eddies and gravitational effects and, as a consequence, random contributions on particle concentration become more important. The contribution of various fluid flow structures and gravity on concentration fluctuations was quantified and explained by quadrant analysis of the cross-correlation between measured particle streamwise velocity and concentration. The calculations of the fluid flow in the shear layer were based on the discrete vortex method and the discrete phase motion was calculated by Lagrangian particle tracking. The calculations showed fluid velocity fluctuations frequency spectra with −5/3 decay, as measured in the experiments, and the simulated particle mean and rms velocities and cross-correlation coefficients of particle concentration and

* Corresponding author. Tel.: +44-20-7594-7057; fax: +44-20-7823-8845.
E-mail address: y.hardalupas@imperial.ac.uk (Y. Hardalupas).

0301-9322/$ - see front matter
doi:10.1016/j.ijmultiphaseflow.2003.07.003

velocity fluctuations agreed qualitatively with the measurements. Remaining discrepancies in the absolute values were due to the omission of gravity in the calculations and the resulting narrower range of fluid flow eddy sizes predicted by the calculations relative to experiments. The consequences of current findings on the operation of light detection and ranging (LIDAR) systems for measurements of atmospheric turbulence due to vortices of the wake of airplanes are discussed and improvements in the data processing are suggested.

Keywords: Shear layer flow; Particle dispersion; Discrete vortex method; Turbulent flow; LIDAR measurement

1. Introduction

In the last twenty years, light detection and ranging (LIDAR) instruments for measurement of the true air speed of aircraft have been developed, e.g. Huffaker and Hardesty (1996). Such sensors have advantages compared to pressure probes, since they are more robust, do not need calibration and could measure the air speed some 10 m away from the aircraft. Such information could warn pilots of presence of clear air turbulence or strong vortices created by other aircraft, especially during landing. The operation of LIDAR systems relies in emitting laser light and detecting on board the aircraft the Doppler shift of the scattered light from aerosols. However, the concentration of aerosols in the atmosphere varies, as well as the size of scattering particles. For example, LIDAR systems must detect scattered light from a few aerosol particles with sizes below 1 μm in dry air, from many small droplets around 10 μm in fog, and from many droplets up to several millimetres when flying through rain. This means that the intensity of scattered light may change by many orders of magnitude, hence it must be attenuated or amplified before processing it to obtain velocity information. In addition, the probe volume size of such systems influences particle concentration and the velocity measured by particle scatterers may not represent the correct fluid velocity. Therefore, there is a need to consider the magnitude of particle concentration fluctuations in the atmosphere, the contribution of atmospheric turbulence or aircraft wakes on such concentration fluctuations, the influence of the probe volume size on detected concentration fluctuations and the correlation between particle concentration fluctuations and particle velocities to provide guidelines to developers of such LIDAR systems.

The existence of temporal and spatial fluctuations of concentration of the dispersed phase in two-phase flows has been observed in many industrial applications, including liquid-fuelled combustors and chemical processes, and occurs due to particle interaction with the continuous phase flow. In addition, particle concentration fluctuations may increase the local particle concentration at levels much higher than the average value and, therefore, modify the carrier fluid turbulence and the resulting mixing process in the flow. However, the experimental quantification of the amplitude of temporal and spatial particle concentration fluctuations has not been achieved, because of limitations of current experimental techniques. An attempt in this direction has been reported in the measurements of particle concentration fluctuations using phase Doppler anemometry (PDA) in two phase pipe flows by Van de Wall and Soo (1994), but the measurements of instantaneous particle concentration depended on a choice of a sampling time, which made the interpretation of the results difficult. For example, Hardalupas and Horender (2000,

2001) showed that the rms of droplet number density fluctuations, measured by PDA, could vary by a factor of 3 by changing the sampling time interval by a factor of 25.

Imaging techniques have also been used to quantify particle concentration fluctuations. However, the choice of interrogation windows on resulting instantaneous images of the particle flow for the measurement of particle concentration can affect the resulting value, in a similar way as the sampling time for the point measurement techniques mentioned above. For example, Longmire and Eaton (1992) used phase-locked digital imaging to measure spatial distribution of particle number density in a pulsed jet laden with glass beads. They found that the instantaneous number density, integrated radially over the jet, had maximum values up to three times larger than the minimum values. The size of the probe volume for concentration measurements was kept smaller than the lengthscale of the observed preferential particle concentration distribution and, therefore, they measured the random and non-random fluctuations of particle concentration. However, the effect of relative size of probe volume was not examined and the contribution of non-random concentration fluctuations was not quantified. Lázaro and Lasheras (1992) and Kiger and Lasheras (1995) measured particle concentration fluctuations in a natural and forced shear layer flow, respectively, laden with a spray by light attenuation of a laser beam placed along the width of the shear layer. However, these concentration fluctuations were spatially averaged and, therefore, only representative of the local particle concentration in the forced flow. Since the natural shear layer flow shows considerable three dimensional structures in the fluid and the particle phase, e.g. Ling et al. (1998), the laser attenuation method can only give measurements for the local particle concentration in the forced shear layer flow, which is nominally two dimensional.

Therefore, few methods are available for measurement of local particle concentration fluctuations and the influence of the size of probe volume on such measurements has not been quantified.

In addition, the correlations of fluid and particle velocities and concentration, as they appear in the modified equation for the turbulent kinetic energy including disperse phase turbulence, e.g. derived by Chen and Wood (1985), have not been completely quantified yet. Only data in jets measured by Prevost et al. (1996), who used phase Doppler anemometer, and Sakakibara et al. (1996), who used imaging techniques, are available. However, uncertainties remain, because of the interpolation procedures, since the fluid velocity could not be measured at the same time and location as the particle velocities. However, correlations that involve particle concentration fluctuations are usually omitted as negligible, although they could be important in the equation describing the carrier phase turbulence modification as:

$$\frac{\mathrm{d}k}{\mathrm{d}t} = \left(\frac{\mathrm{d}k}{\mathrm{d}t}\right)_{\mathrm{sp}} - \frac{\bar{C}}{\rho_{\mathrm{f}}\tau_{\mathrm{p}}}\left(\overline{u_{i\mathrm{g}}u_{i\mathrm{g}}} - \overline{u_{i\mathrm{g}}u_{i\mathrm{p}}}\right) - \frac{1}{\rho_{\mathrm{f}}\tau_{\mathrm{p}}}\left(\overline{cu_{i\mathrm{g}}u_{i\mathrm{g}}} - \overline{cu_{i\mathrm{g}}u_{i\mathrm{p}}}\right) - \frac{1}{\rho_{\mathrm{f}}\tau_{\mathrm{p}}}\left(\overline{U_{i\mathrm{g}}} - \overline{U_{i\mathrm{p}}}\right)\overline{cu_{i\mathrm{g}}}. \tag{1}$$

In addition, the non-random particle concentration fluctuations are not considered in the above equation and such components may be significant. In Eq. (1), overbars denote time-averaging, capital letters mean flow quantities, lower case letters fluctuating components, subscript '*i*' the component of the co-ordinate system, subscripts 'g' and 'p' indicate fluid/gas and particle quantities respectively, c the particle mass concentration, u denotes velocity and τ_{p} is the particle relaxation time, 'sp' means single phase.

Longmire and Eaton (1992) identified the strongly organised fluid flow structures, as responsible for particle dispersion, rather than diffusion due to random three-dimensional turbulence. However, their flow was strongly organised due to pulsation, which increased the energy of specific flow structures, which is not occurring in unforced shear layers. They found that particle clusters formed because particles are dispersed into distinct axial regions from upstream and downstream locations due to the fluid flow and particles did not disperse by diffusion away from areas of high concentration. Their combined velocity and concentration measurements were phase-locked to the forced flow and, therefore, obtained ensemble-averaged correlations of particle velocity and concentration, which could be combined to obtain a flux measurement, which explained the particle-flow interaction mechanism. However, gravity acted in the main flow direction of their jet flow and did not directly contributed to the cross-stream dispersion of particles, which is examined in the current study.

Lázaro and Lasheras (1992) and Kiger and Lasheras (1995) measured correlations between particle concentration and velocity in their shear layer flow. However, in the unforced flow conditions the measured particle concentration fluctuations could be affected by spatial averaging, while the velocity measurements were spatially resolved and, therefore, the two quantities were not necessarily associated with the same region of the flow. In addition, many droplet sizes were present in their spray and, therefore, the influence of different Stokes numbers on droplet dispersion and preferential concentration could not be isolated. Finally, the effect of gravity was not considered in their analysis of particle dispersion, and gravity is expected to have different consequences on particle dispersion in the current flow.

Sato (1995) included fluid velocity and particle concentration correlations in predictions of two-phase flow using a multi-timescale model and found that the trends of carrier phase turbulence modification due to particles were predicted better, when particle concentration fluctuation effects were included. However, this work assumed random particle concentration fluctuations and neglected the two way coupling of vortical fluid flow structures and particle centrifuging leading to preferential concentration, which happens in isotropic turbulence due to energy-containing eddies (e.g. Fessler et al., 1994), or in anisotropic turbulence due to large scale flow structures (Crowe et al., 1988).

Crowe et al. (1996, 1997) described how large scale eddies of the continuous phase flow can influence droplet dispersion and lead to preferentially increased concentration of the disperse phase between the flow eddies. The droplet response to fluid turbulence was quantified in terms of Stokes number, defined as ratio of droplet response time scale to the relevant fluid flow timescale, and the centrifuging effect is maximised when the Stokes number based on the time scale of coherent flow eddies is around unity. This clustering of particles may increase the influence of particles on the turbulence structure of the carrier fluid. Chung and Troutt (1988) and Tang (1990) presented results of particle dispersion in shear flows using discrete vortex methods to model the fluid flow. However they did not use an analytically appropriate formula including the viscosity of the fluid flow, and, hence their model could not produce a proper turbulent spectrum. In addition, they did not consider the gravitational effect on particle dispersion. However, they could predict preferential concentration of particles due to large scale structures, which agreed qualitatively with DNS calculations (Ling et al., 1998), but they did not quantify mean and fluctuations of particle concentration and the resulting cross-correlation terms of particle concentration and velocities, in order to assess the ability of the discrete vortex models to predict measured quantities.

The purpose of the experimental part of the work is to present a planar imaging technique for measurement of simultaneous particle concentration and velocity, based on digital images recorded using a particle image velocimetry (PIV) system, and apply it to measure particle velocity and concentration correlation terms, such as those appearing in Eq. (1), which involve concentration fluctuations of the disperse phase in a plane shear layer. These results are subsequently considered in terms of the accuracy of LIDAR fluid velocity measurements in the atmosphere. The measurement of the rms of particle concentration fluctuations is affected by the size of the interrogation cell on the measured images and this effect is quantified to assess the lengthscale of particle concentration distribution associated with non-random fluctuations. The effect of the size of the interrogation cell has not been considered in previous experimental studies and, as a consequence, previously reported correlations between particle concentration and velocity may not have been measured appropriately to allow comparison with numerical results. The turbulent mass flux of particles, i.e. cu_p, which must be modelled in two-fluid numerical approaches, e.g. Chen and Wood (1985), is quantified and analysed by quadrant analysis to identify the contribution of different flow structures and gravity to the overall value. The results quantify the contribution of non-random fluctuations to the mean particle concentration and consider the effects of gravity and inertia on particle dispersion. An important difference from previous studies is that the particles are injected at the low speed side of the shear layer, which enhances the influence of gravity on particle dispersion and allows to quantify the effect of particle centrifuging on particle dispersion, while is acting against gravitational effects. This is explained further in the discussion of the results.

The purpose of the two-phase calculations of the reported work is to present mean and rms of fluctuations of velocity and concentration, based on a discrete vortex method, and assess the ability of this approach to quantify the cross-correlations of particle concentration and velocity fluctuations and particle streamwise and cross-stream velocity. Calculations of these quantities have not been presented in the literature.

The paper presents the experimental arrangement and PIV instrumentation and data processing in Section 2, followed by the numerical approach, based on the discrete vortex method that satisfied the non-viscous vorticity transport equation, in Section 3. Section 4 presents the experimental results, compares with the calculated quantities and discusses the findings in terms of previous work and the consequences for the operation of LIDAR systems. The paper ends with a summary of main conclusions.

2. Experimental set-up

2.1. Wind tunnel set-up

A wind tunnel was set up horizontally to produce a shear flow laden with glass beads, Fig. 1. A 2.4 kW radial fan blower delivered the air flow, which passed through a pressure drop and after that a 1.8:1 contraction. An aluminium splitter plate with initial 1.5 mm thickness was placed within the contraction and gradually was reduced to around 0.5 mm at the edge. The plate was bend towards the low speed side (Fig. 1), so that the flow streamlines at the high speed side of the tunnel remained parallel to the surface at the beginning of the plate. A filter was mounted at the

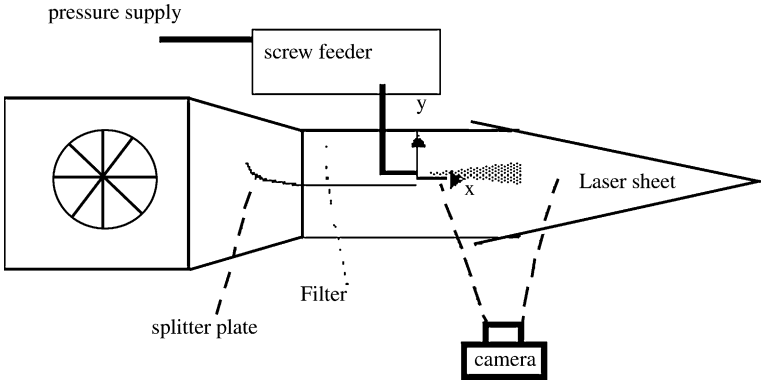

Fig. 1. Experimental arrangement of the wind tunnel and the particle image velocimeter system.

low speed side of the plate (upper side of Fig. 1) to adjust the low speed air flow and ensure flow uniformity. The test section was square with dimension of 300 mm, and the splitter plate was located at its centre and was 300 mm long.

The beads were metered by a screw feeder, which was placed in a closed, pressurised box, before they were injected into the flow. The fluctuations of particle concentration were around 15% of the mean particle concentration at the injector exit, which were caused by the operation of the screw feeder. To avoid agglomeration, a hydroscopic gel was added to the hopper, which supplied the glass beads. No electrostatic effects on particle dispersion were observed and, therefore, no special measures had to be taken. Two size ranges of glass beads 40–70 μm and 70 –110 μm (SOVITEC GmbH, Saarbrücken, Germany) were used and will be referred to as 55 and 90 μm glass beads. The glass beads were injected through a pipe with inner diameter 5 mm located at the end of the splitter plate at the low speed side of the flow with the centre of the pipe located 3 mm above the splitter plate. PIV measurements at the exit of the pipe showed that the streamwise velocity of the particles was 3 m/s and the rms of streamwise and cross-stream velocity fluctuations 0.2 m/s for each component. The local mass loading was estimated 9% and 12% for the 55 and 90 μm particles respectively. The test section ended in a large plastic sac, around 3 m high, with holes allowing the decelerated air flow to escape, while nearly all glass particles were collected at the bottom of the sac.

Fig. 2 shows the resulting fluid flow profiles measured using laser Doppler anemometry for the streamwise mean and rms velocity for distances $x = 10$ mm and 100 mm downstream of the end of the splitter plate. The streamwise velocity was 5.5 m/s on the high speed side and 0.8 m/s on the low speed side, and the turbulence intensity on the undisturbed high speed side was around 3%, which is similar to the flow used by Lázaro and Lasheras (1992). The Reynolds number of the flow based on the momentum thickness of 52 mm at $x = 250$ mm, the location where the particle flow characteristics were studied, and the velocity difference was around 20,000. Tennekes and Lumley (1972) presented an analysis to estimate the Reynolds number based on the integral and Taylor time scale of the flow as:

$$Re = 15 \cdot \left(\frac{t_{\text{int}}}{t_{\text{Taylor}} \cdot A} \right)^2, \tag{2}$$

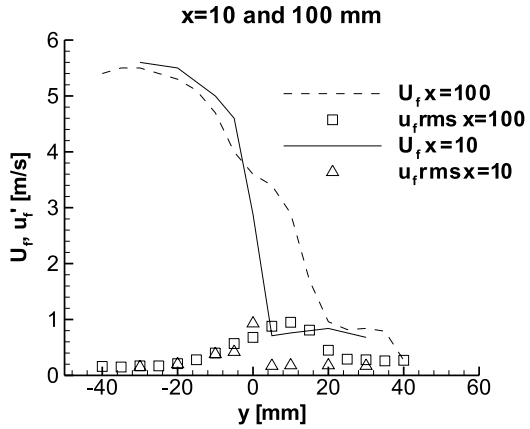

Fig. 2. Streamwise mean and rms of fluctuations of fluid velocity profiles at streamwise distances $x = 10$ and 100 mm downstream of the end of the splitter plate, measured using laser Doppler anemometer (LDA).

t_{int} denotes the integral time scale of the flow, t_{Taylor} the Taylor microscale, which is estimated as the time where a parabola that has the same curvature as the velocity autocorrelation function meets the time axis, see Fig. 3. A is a constant of the order of unity. Estimating the integral eddy time scale, based on the momentum thickness and the velocity difference at $x = 100$ mm, t_{int} was 12 ms. With t_{Taylor} 0.4 ms, as extracted from Fig. 6, and $A = 1$, the Reynolds number was 13,500, according to Eq. (2). This analysis will also be used to evaluate the Reynolds number in the vortex blob calculation, since the numerical fluid viscosity is not known for the calculation of the Reynolds number using the velocity and typical dimension of the flow.

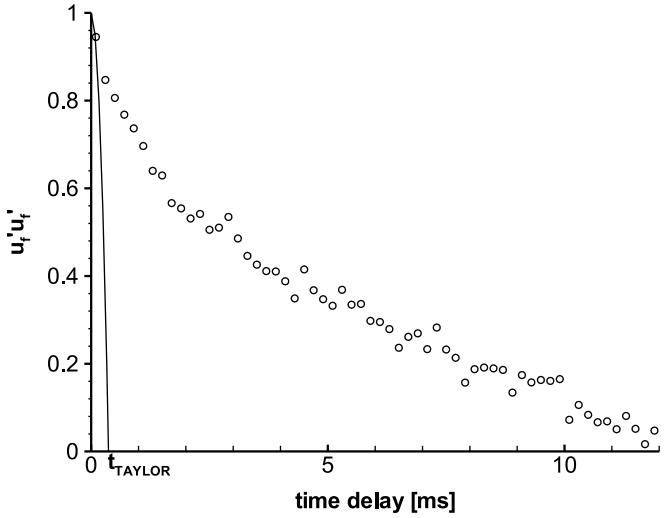

Fig. 3. Measured normalised autocorrelation function of streamwise velocity at $y = 300$ mm and $x = 10$ mm with parabola matching at time delays 0 and 0.1 ms.

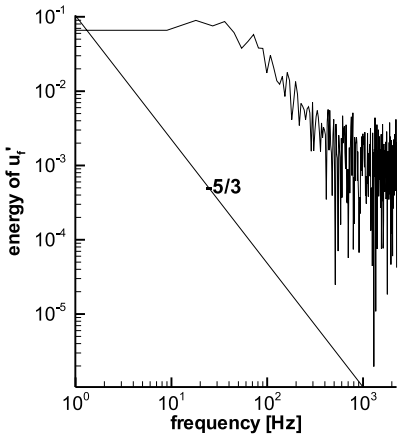

Fig. 4. Measured frequency spectrum of fluid streamwise velocity at position $x = 100$ mm, $y = 0$ mm.

Fig. 4 presents a frequency spectrum of the streamwise velocity at position $x = 100$ mm and $y = 0$ mm. The spectrum was obtained by fast Fourier transformation of the autocorrelation function of the velocity, measured with laser Doppler anemometer with resolution of 0.2 ms. Increased energy of the fluctuating velocity could be observed over a range of frequencies between 10 and 100 Hz due to the large scale structures and the shape of the spectrum shows the $-5/3$ decay for higher wave numbers, as expected for a turbulent flow. This is in agreement with the integral timescale of the flow of 12 ms at position $x = 100$ mm, while the frequency of convected large flow structures is expected to be lower than that of the integral scale.

An assessment of the particle behaviour to the fluid flow is presented here. Table 1 shows the particle response times and the terminal velocity for the size range of 55 μm particles (40–70 μm) and the 90 μm particles (70–110 μm) for two streamwise distances from the splitter plate, $x = 100$ and 250 mm. The influence of particle inertia on particle dispersion is quantified by the Stokes number, defined as the ratio of particle relaxation time and time scale of large eddies. The gravitational effect is evaluated by the gravitational settling parameter, defined as the ratio of particle terminal velocity and flow velocity. Mean and turbulent flow settling parameters can be defined, associated with the mean and turbulent flow velocity. Table 2 shows the range of particle Stokes numbers and mean and turbulent settling parameters for 55 and 90 μm particles at two streamwise positions from the splitter plate, 100 and 250 mm corresponding to a region close to the splitter plate and the locations where measurements of particle characteristics were obtained. The particle response to the large eddies improves with downstream distance, since the period of the convection of large eddies was 40 and 65 ms, as indicated by the measured frequency spectra,

Table 1
Particle response time and terminal velocity

Particle response times (ms)					Particle terminal velocity (m/s)				
40 μm	55 μm	70 μm	90 μm	110 μm	40 μm	55 μm	70 μm	90 μm	110 μm
11.6	22	35.6	58	86.6	0.11	0.21	0.34	0.57	0.70

Table 2
Particle Stokes numbers and gravitational settling parameters

Streamwise location (mm)	Flow time scale (ms)	Range of particle Stokes numbers		Range of mean flow settling parameter		Range of turbulent flow settling parameter	
		55 μm	90 μm	55 μm	90 μm	55 μm	90 μm
100	40	0.3–0.9	0.9–2.1	0.11–0.34	0.34–0.70	0.22–0.68	0.68–1.4
250	65	0.2–0.6	0.6–1.4	0.11–0.34	0.34–0.70	0.22–0.68	0.68–1.4

at 100 and 250 mm respectively. Gravity acted normal to the main flow direction and the particle gravitational settling parameter was based on mean and turbulent flow velocity of 1 and 0.5 m/s respectively, corresponding to values at the low speed side of the shear layer. This choice was due to the interest to evaluate the importance of gravity on particle dispersion for particles present on the low speed side of the shear layer. Table 2 shows that the 55 μm particles at 250 mm had a range of Stokes numbers between 0.2 and 0.6 and 90 μm particles between 0.6 and 1.4. Therefore, it is expected that the 55 μm particles are more responsive to the flow and 90 μm particles should demonstrate particle centrifuging due to the large flow structures. Also, gravity is expected to have an influence on particle dispersion and assist particles to disperse away from the low speed side of the shear layer, since the mean flow settling parameters were around 0.2 and 0.5 and the turbulent settling parameters were around 0.5 and 1 for the 55 and 90 μm particles respectively. Particle centrifuging from large eddies due to inertia can disperse particles against gravity from the high speed to the low speed side of the shear layer.

2.2. The PIV system

The particle image velocimeter (PIV) system comprised a double pulse Nd:YAG laser with energy 45 mJ per pulse of length 8 ns, which created a laser sheet of 1 mm thickness, and a 12 bit camera which allowed to obtain two consecutive images with a time delay of 200 μs. A lens with focal length 100 mm and aperture 8 was mounted in front of the camera. The particle velocities were derived by the cross-correlation method for interrogation windows of size 32×32 pixels, see Raffel et al. (1998), which corresponded to 3.2 mm $\times$ 3.2 mm in the current flow. The measurements for each interrogation window were validated on the basis of the magnitude of the correlation peak and the resulting velocities had to give smooth gradients to the neighbouring interrogation windows. 400 images were recorded for all flow parameters and the results of the single images were averaged for each correlation window to measure the local mean and rms particle velocities. The number of images was limited by computer storage capacity, but it was larger than the number of images used in previous work, i.e. 25 images for the work of Longmire and Eaton (1992). This led to increased uncertainties, which are quantified later in the section. It should be noted that uncertainties exist when applying a cross-correlation method for measuring mean and rms velocities of inertia particles. Usually, it is assumed that tracer particles behave as a continuum and their velocity changes only little in one interrogation window. This is not valid for the glass beads of the present work, however the objective of the present work is to measure particle cloud velocities and concentration rather than the velocity of individual particles, e.g. Soo (1990).

As a measure of particle concentration c the particles were counted in each interrogation window by means of image processing. In each interrogation window, cross-correlation processing derived the velocity and the number of particles was counted, using the image processing software OPTIMAS. A particle was identified, when a pixel showed an intensity value larger than a threshold, and a particle was allowed to have sizes above one pixel. The glass bead size was assumed uniform and the gain of the system was adjusted, so that only glass beads larger than a certain size could only be identified, to avoid detection of any smaller particles present in the air flow. PIV images were recorded and processed to measure fluctuating particle concentration in the entire flow field by dividing the images into small cells and calculating the rms of fluctuations of the number of particles in each cell, Fessler et al. (1994). A parameter D called deviation from randomness was defined as

$$D = \frac{\sigma - \lambda^{1/2}}{\lambda} \tag{3}$$

with σ being the measured rms and λ the mean number of particles per cell. If the particles were randomly distributed, the number of particles per cell would follow a Poisson distribution and the rms would be equal to the square root of the mean and, therefore, D would become zero. Hence, D represents a measure of the deviation of particle distribution from randomness, normalised by the mean particle concentration, and is evaluated for different cell sizes for the entire flow field. The cell size leading to maximum deviation from randomness represents a length scale of the particle flow associated with non-random (preferential) concentration.

Correlation of particle fluctuating velocities and concentrations were computed from the instantaneous images after subtracting the normalised mean values, according to

$$\overline{cu_{\mathrm{p}}} = \frac{\overline{c(t)u_{\mathrm{p}}(t)}}{\overline{c^2(t)}^{1/2}\overline{u_{\mathrm{p}}^2(t)}^{1/2}} \tag{4}$$

providing the normalised correlation coefficients. Quadrant analysis of the correlated data provided information on the flow structures responsible for the average value of the cross-correlation coefficient at different locations in the shear layer.

The statistical uncertainties of the measurements were determined according to Yanta and Smith (1978) for 95% confidence level and typical values of the measurements. The uncertainties were 2% and 7% for the mean and rms of fluctuations of particle velocity, 6% and 10% for the mean and rms of fluctuations of particle concentration, 15% for the cross-correlation between the cross-stream and streamwise velocity fluctuations and 20% for the cross-correlation terms between particle velocity and concentration fluctuations.

3. Numerical simulation technique

A computer programme based on the discrete vortex method was developed to calculate the shear layer flow. The mathematical basis of the method is to satisfy the non-viscous vorticity transport equation

$$\frac{D\omega}{Dt} = 0 \tag{5}$$

by tracking vortices to compute instantaneously the fluid development in a free shear layer flow. The vortex blob method was used, as reviewed by Leonard (1980) or Sarpkaya (1989), which avoids singularities for the case that vortices get close together, leading to infinitely large velocities. The equations describing the velocities read as follows:

$$u(x,y) = \left(-\frac{1}{2\pi} \sum_{i=1}^{N} \Gamma \frac{y - y_i}{|\vec{r} - \vec{r}_i|^2 + b^2} \right) + u_{\text{convect}}, \tag{6}$$

$$v(x,y) = \frac{1}{2\pi} \sum_{i=1}^{N} \Gamma \frac{x - x_i}{|\vec{r} - \vec{r}_i|^2 + b^2}, \tag{7}$$

$r = (x, y)$ is the two-dimensional space vector and the velocity vector is (u, v). The constant factor b in the denominator is referred to as vortex blob size in the literature and represents a numerical fluid viscosity without dissipating energy. b was set to 0.35 times the initial distance of vortices located at the splitter plate following initial tests. The inflow boundary conditions for the generation of a free shear flow were satisfied by adding vortices on the virtual splitter plate at an initial distance between point vortices of 1.25 mm and release them at the end of the plate. The vortex strength Γ was set, so that the velocity difference between the two streams of the shear layer was 4 m/s and u_{convect} was 1 m/s. The outflow boundary conditions were satisfied in a similar way as the inflow, by adding vortices along the direction of the flow at locations larger than the region of interest, which was $x = 800$ mm in the presented results. Fig. 5 illustrates the flow pattern of the pairing vortices in the shear flow with the vortices shown as rings. The graph additionally shows dispersed 90 μm particles that were tracked through the flow considering aerodynamic force simplified as Stokes drag, leading to equation of motion for a single particle as

$$\vec{u}_{\text{p}} = \vec{u}_{\text{p}} + (\vec{u}_{\text{f}} - \vec{u}_{\text{p}}) \cdot (1 - \mathrm{e}^{-\Delta t/\tau_{\text{p}}}). \tag{8}$$

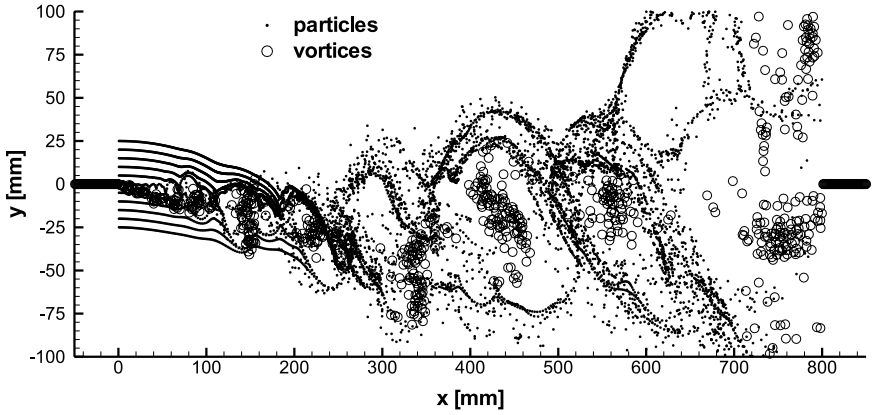

Fig. 5. Simulated dispersion pattern of the fluid vortices and the 90 μm particles at one instant of time. Flow direction is from left to right.

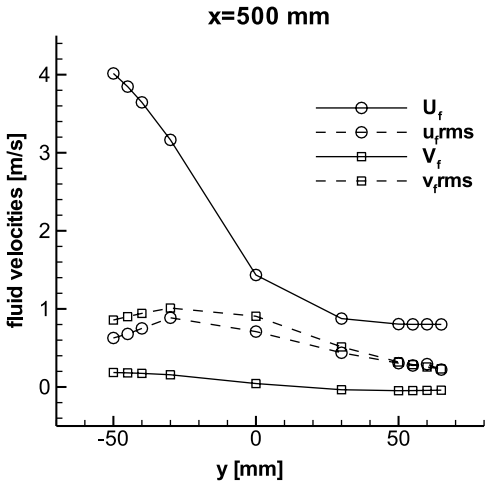

Fig. 6. Simulated fluid velocity profiles in the shear flow at streamwise position $x = 500$ mm.

This description was applied in our case, assuming that particle Reynolds number was of the order of unity. The effect of gravity was not considered.

Fig. 6 shows profiles of the mean and rms of fluctuations of streamwise and cross-stream fluid velocities in the simulated shear flow at $x = 500$ mm downstream of the end of the splitter plate. The rms of the fluctuations of the velocities was large at locations with high mean flow gradients of the streamwise velocity component and the rms of the cross-stream component was larger than that of the streamwise component. However, this is attributed to the assumption of two-dimensional flow. For Taylor microscale of 2.5 ms and integral scale 25 ms, both derived from the corresponding streamwise velocity autocorrelation function, the Reynolds number in the simulations was 1500, according to Eq. (2). This estimate of the resulting Reynolds number in the calculations is not usually presented in the literature and, therefore, comparison with previously reported calculations cannot be achieved.

Fig. 7 shows the frequency spectrum from the simulation of the streamwise velocity as a function of time at location $x = 500$ mm and $y = 0$ mm in the shear flow. A maximum in the energy spectrum was observed for low frequencies around 10 Hz, which was associated with a fluid flow time scale of 100 ms. However, the decay of the energy for higher wave numbers did not perfectly follow a $-5/3$ law. Hence, tests were made with different core shapes and the vortex core growing in time, so that the viscous transport equation could be satisfied. In this way, the calculated spectrum of the velocity fluctuations approached the measured spectrum, presented in Fig. 4, which indicates that this model including a correct description of viscosity, see e.g. Leonard (1980) and Shiels (1998) should be used for the simulations. However, the exponential decay of the vortex core led to smaller far field influence of the vortices, which meant that outflow boundary conditions could not be satisfied correctly.

The time dependent particle concentration was defined by the number of particles contained in a probe volume for every time step of the calculation. If there was more than one particle in the probe volume, the particle velocity was not averaged, but every particle event was treated as a single measurement and counted for computation of particle mean and rms velocity.

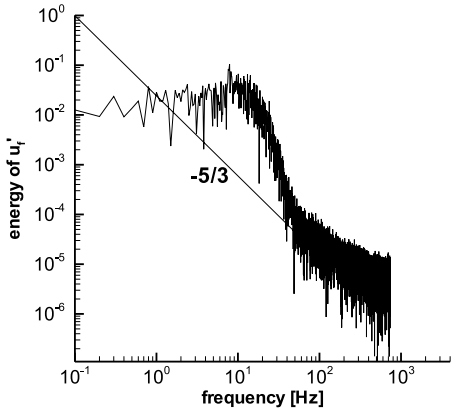

Fig. 7. Frequency spectrum of the simulated streamwise velocity at position $x = 500$ mm, $y = 0$ mm.

4. Results

The length scale of preferential concentration of particles was quantified by the method described in Section 2.2 for the particle flow captured by the PIV system, in a region downstream of the splitter plate between $x = 200$ and 320 mm and between cross-stream directions $y = -40$ to +40 mm. The normalised parameter D, defined by Eq. (3), was calculated for a range of interrogation window sizes and is shown in Fig. 8. The size of the region of interest (interrogation window) for which the deviation from randomness is largest corresponds to the length scale of preferential concentration of particles. However, it should be noted that the current fluid flow is non-homogeneous, hence the parameter D is a function of streamwise and cross-stream position, as shown later in Fig. 9(d). The consequence of this on the spatially averaged length scale of preferential concentration is discussed later in the text.

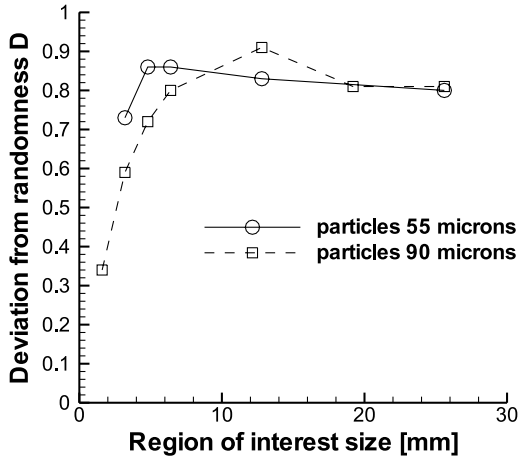

Fig. 8. Measurement of the spatially-averaged deviation from randomness of particle concentration for 55 and 90 μm particles as a function of the size of region of interest in mm, representing the size of a square probe volume interrogation cell. Location in the shear flow between $x = 210$ and 310 mm and $y = -40$ and 40 mm.

In the measured particle distribution, the length scale of preferential concentration was 6.4 mm for the 55 μm particles and 12.8 mm for the 90 μm particles. Therefore, it was assured that by using interrogation windows of 32×32 pixels, representing 3.2×3.2 mm, for the measurement of the particle velocity and the corresponding correlations of particle velocity-concentration fluctuations the large scales of the particle flow could be resolved. The intensity of particle concentration fluctuations corresponds to the maximum value of D in Fig. 8, which was around 0.8 of the mean particle concentration. In a channel flow laden with different particle sizes, Fessler et al. (1994) measured maximum deviation from randomness D of around 0.4, which is 50% less compared to the current experiment. However, the current flow was inhomogeneous and the value of D varies with the location in the flow, as shown later in Fig. 9(d). Therefore, the spatially averaged value across the shear layer cannot be directly compared with the results of Fessler et al. (1994), which were in a nominally homogeneous flow.

The associated lengthscale of preferential concentration of 6.4 and 12.8 mm for maximum non-random particle concentration fluctuations of 55 and 90 μm beads is about 0.15 and 0.25 of the local shear layer width and indicates the clustering of particles between fluid eddies, associated

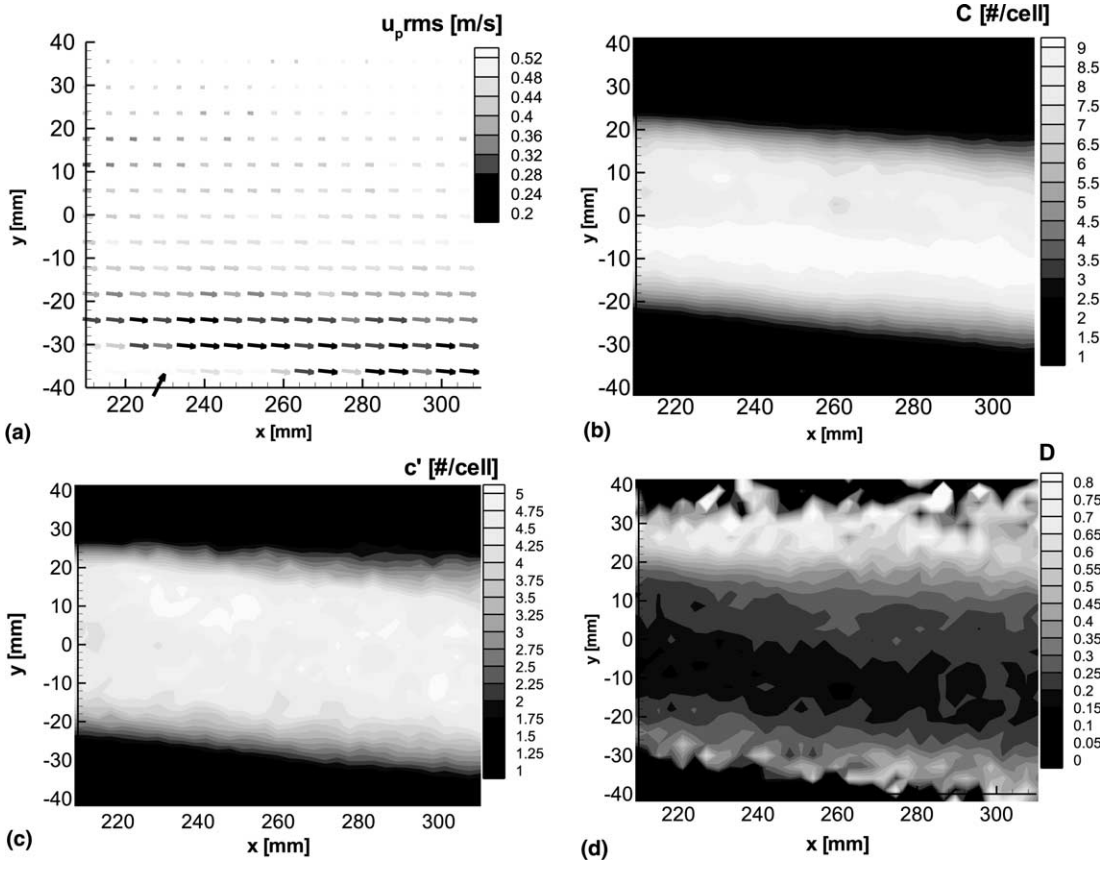

Fig. 9. Measurement of particle characteristics for 55 μm glass beads. (a) Particle velocity field, (b) particle mean number density (number per 3.2×3.2 mm^2 cell), (c) rms of fluctuations of particle number density and (d) spatially resolved deviation from randomness D of particle number density fluctuations.

with particle centrifuging. It should be noted that the ratio of shear layer width to vortex spacing is approximately one, as derived from the shadowgraph images of Brown and Roshko (1974) and Bernal and Roshko (1986). Hence, the shear layer width is similar to the lengthscale of the local large scale vortices. The larger lengthscale of preferential concentration of the 90 μm particles compared to the 50 μm is justified by around unity Stokes number for the larger particles, which suggests stronger particle centrifuging by the large vortices relative to the 55 μm particles. In addition, the effect of gravity is higher for the 90 μm particles and tends to disperse particles away from the low speed side of the shear layer, which will also increase the lengthscale of the non-random concentration fluctuations. Particle centrifuging for the 90 μm particles is in agreement with the observations of the calculations of Fig. 5, which shows that particles tend to concentrate between and at the edge of fluid vortices in a limited region, which is a fraction of the local shear layer width. Fessler et al. (1994) measured lengthscale of maximum preferential concentration around one tenth of the channel width for particles with largest D, which is smaller than for the current experiment. However, in their experiment the lengthscale of the flow structures was smaller than the channel width and direct comparison cannot be made.

In Fig. 9, measured quantities of the 55 μm particles for the entire flow field are presented. Fig. 9(a) shows the mean velocity vectors of the particle flow phase and the rms of the streamwise velocity component as grey levels of the vectors. It should be noted that the particle concentration was low for y locations above and below ±25 mm, hence velocity measurement uncertainties increased at those positions. A small downward velocity component can be observed due to gravity and the rms of the streamwise particle velocity component around the centre of the shear layer increased by around 10% with increased streamwise distance. This may happen due to particles being able to follow partly the air flow velocity fluctuations and the contribution of gravity to particle dispersion, as discussed later in the text. Fig. 9(b) and (c) show the mean number of particles per interrogation window and the rms of particle number in these cells. The location of the maximum mean and rms of fluctuations of particle concentration moved downward with increased streamwise distance due to gravity. It can be seen that the rms of the concentration fluctuations normalised by the mean concentration was around 0.5 at the position, where most of the particles were located, $y = -10$ mm and $x = 220$–280 mm. Kiger and Lasheras (1995) found smaller normalised fluctuations up to 0.3 in their forced shear layer flow, which was laden with a spray comprising a wide range of droplet sizes. A small contribution to the increased normalised particle concentration fluctuations in the current experiment could be the initial 15% particle concentration fluctuations at the injection location. Although these fluctuations would attenuate during particle motion towards the measurement location, which was around 250 mm downstream of the injection location, some concentration fluctuations would still remain in the flow to increase the measured fluctuations, although that could not explain the observed 20% difference between the two experiments. The polydisperse droplet size distribution of Kiger and Lasheras (1995) could lead to reduced preferential concentration and, as a consequence, reduced concentration fluctuations, since very small or very large droplets could penetrate at the centre of the vortical structures, either by following the fluid flow or not interacting at all with the fluid flow respectively. However, it is more probable that the observed difference is due to gravitational effects on dispersion. Their flow was uniformly laden at the high speed side with the spray, which was different compared to the current particle injection at the low speed side. Therefore, in the current flow, gravity could disperse particles from the low speed towards the high speed side and

contribute to increased concentration fluctuations in the shear layer flow, while in the flow of Kiger and Lasheras (1995) the particles would move away from the shear layer due to gravity.

The fact that particle injection in the current flow was from a point source does not influence significantly the particle dispersion characteristics, since the dispersion mainly occurs in the cross-stream direction rather than in spanwise direction, as found by Ling et al. (1998) in DNS calculations and verified by visualisation of the particle distribution in the spanwise direction in the current experiments. Therefore, dispersion in the spanwise direction was much smaller than in the plane of the large vortex structures and, hence, had limited contribution to particle dispersion behaviour.

Fig. 9(d) shows the spatially resolved distribution of the deviation from randomness of the particle concentration fluctuations D for each interrogation window of size 32×32 pixels. It can be seen that D varies between 0.1 and 0.75 for cross-stream locations close to maximum particle concentration at the centre of the shear layer and the edge of the shear flow respectively. This shows that the preferential distribution of the particles is more pronounced at the edge of the shear layer than in the central region, where most of the particles are located. Therefore, the spatially averaged value of D, which was around 0.8 (Fig. 8), is mainly affected by the large fluctuations at the edge of the shear layer and may give misleading impression of overall large deviation from randomness of the particle concentration in the shear layer flow. This explains the difference between the current spatially averaged value of D of 0.8 across the shear layer and the value of 0.4 of Fessler et al. (1994) in a channel flow, which is close to the deviation from randomness D in the central region, where most of the particles are present. This suggests that the influence of the large vortical structures in the central region of the shear layer flow, led to limited non-random concentration fluctuations. The increased non-random fluctuations at the edge emphasises particle centrifuging, which is achieved against gravity for the low speed side of the shear layer (positive y).

Fig. 10 shows scatter plots of the turbulent mass flux cu_p for three cross-stream locations ($y = 20$, 0, -20 mm) to identify important flow events that contribute to the average correlation

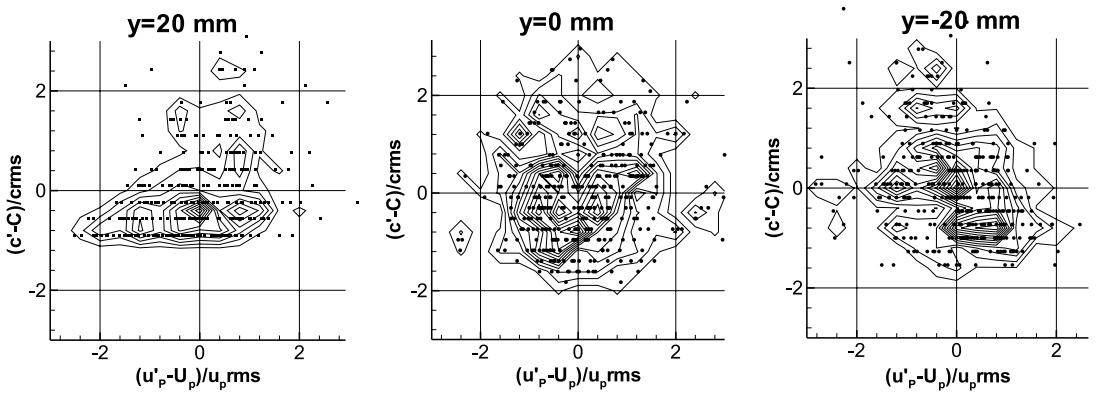

Fig. 10. Scatter plots of the particle velocity and concentration fluctuation events at streamwise position $x = 250$ mm for three cross-stream positions for 55 μm particles, which allows quadrant analysis for the average value of the cross-correlation coefficient. Lines of constant values of the joint probability density functions of the correlated quantities are superimposed on the graphs.

coefficient of particle concentration-velocity fluctuations. Lines of constant values of the joint probability density functions of the correlated quantities are superimposed on the graphs to assist the reader with the following discussion. It should be noted that the values for the normalised concentration are not uniformly distributed, since the particle concentration is measured as integer number of particles in each interrogation window. Therefore, the negative values of concentration are truncated for values of a single particle present in the interrogation cell. It is interesting to note that the number of events were not located equally in each quadrant. The quadrants are identified as follows. Quadrants 1 and 3 correspond to $+c/+u_p$ and $-c/-u_p$ and lead to positive correlation and quadrants 2 and 4 to $+c/-u_p$ and $-c/+u_p$ respectively and lead to negative correlation. The flow field indicated that the particles were centrifuged by the flow structures and this structure will assist to explain the observed scatterplots of fluctuations of particle concentration and velocity.

At location $y = 20$ mm, the low speed side of the shear layer, the average correlation cu_p is positive, because most events are located in quadrants 1 and 3, which corresponds to particles with velocity and concentration higher or lower than the mean. This is justified by particle centrifuging by the fluid large scale vortices mechanism that disperses large number of particles with high velocity to the low speed side (quadrant 1). When a large scale fluid vortex has been convected downstream, low velocity particles with low concentration remain (quadrant 3). The concentration of particles is reduced after the crossing of the large eddies due to particle dispersion away from the low speed side due to gravity.

For position $y = 0$ mm, events of correlated u_p and c_p are nearly uniformly distributed over all quadrants, leading to correlation close to zero, since for positions close to the centreline the probability of observing all events is similar. Gravity may be assisting particle dispersion and justifying the presence of low speed particles in the central region. This effect is explained in detail in the next paragraph. For position $y = -20$ mm, most of the events are located in quadrant 4 and fewer in quadrant 2, whereas in the other quadrants there are much less events. This is justified by gravitational (discussed in the following paragraph) and particle centrifuging effects which disperse large number of particles with low velocity away from the low speed side of the shear layer (quadrant 4). When a large scale fluid vortex has been convected downstream, high velocity particles with low concentration remain (quadrant 2).

Particle centrifuging from high and low speed side is happening at different times relative to the crossing of a large scale structure at each streamwise distance. However, there is time between the convected flow eddies with period of 65 ms at 250 mm streamwise distance, for gravity to play a role on particle dispersion from the low to the high speed side of the shear layer. The large flow structures are approximately 80 mm wide at 250 mm streamwise distance and are convected with a velocity of around 4 m/s. Therefore, it takes approximately 20 ms ($= 0.08$ m/4 m/s) for the flow structures to cross at this streamwise distance, while they appear every 65 ms. There is, therefore, a period of 45 ms during which particles could move due to gravity from the low to the high speed side, because of their limited response to the smaller fluid flow eddies. Considering the terminal velocity of 55 and 90 μm particles of 0.21 and 0.57 m/s (Table 1), the particles will move normal to the main flow direction due to gravity by around 10 and 26 mm respectively, which is a large portion of the shear layer width, between the large fluid flow eddies. Therefore, it is possible for low speed particles to disperse in the central region and the high speed side of the flow due to the gravity. Gravitational particle settling parameters (Table 2) were found important for turbulent

dispersion of particles and the mean concentration profiles of Fig. 9(b) indicate increased particle concentration at the high speed side of the flow confirming the above suggestion. Therefore, gravity is partly responsible for the presence of low speed particles with high concentration at the high speed side of the flow.

The current findings have some consequences for LIDAR applications for measurement of turbulence in the atmosphere, in particular velocity fluctuations associated with the vortices from wakes of airplanes, which may contribute to increased airport capacity and aircraft safety. It is suggested that an additional measurement of the correlation between fluctuations of scattered light intensity (as a measure of particle concentration fluctuations) and measured velocity fluctuations is obtained during LIDAR operation for velocity measurement. If this correlation is non-zero, it indicates that the measured LIDAR velocity does not accurately represent the fluid flow velocity and, therefore, there is a bias in the measurement of atmospheric turbulence. In the presented case, for example at position $y = -20$ mm, this would mean that the velocity measurement is biased towards larger velocities, due to the centrifuging of the scattering particles by the fluid flow.

Fig. 11(a) and (b) show cross-stream profiles of mean and rms streamwise and cross-stream velocities at position $x = 250$ mm for particle sizes 55 and 90 μm respectively. Little difference can be observed in the particle velocities for different sizes. The increase of rms velocities at the edge of the measurement area ($y = \mp 40$ mm) is due to low number of particles in each interrogation window, which increased the statistical uncertainties. However, at cross-stream positions around $y = -30$ mm, the larger particles tend to move slower by around 5%, compared to the smaller particles, which is due to the larger inertia of the larger particles, which need longer distance to be accelerated to the surrounding air flow. For both sizes, the rms velocities of both components are smaller for negative y positions than for positive, because particles at positive cross-stream positions are more likely to have been dispersed by the fluid large-scale structures against gravity.

It should be noted that the PIV correlation method averages the particle velocities within an interrogation cell based on a dominant peak and ignores outliers. This means that particle velocity variations occurring at small scales and variations caused by particle trajectories with differing histories are suppressed. Using the numerical simulations presented above, it was estimated that single particle velocities in the interrogation cell at an instant in time could vary up to 50% of the measured time-averaged rms value of the particle velocity fluctuations at that location. Hence, it is expected that the rms of particle velocity fluctuations be biased towards smaller values by the averaging process within the interrogation cell of the PIV system. More work is required to quantify this bias for various flow conditions. However, this measurement approach represents the averaging process of a LIDAR system, which has a probe volume with the same relative size to the local scale of the flow. This emphasises the need to evaluate the effect of the relative size of the probe volume to the flow lengthscale on the LIDAR velocity measurement.

In Fig. 11(c) and (d) cross-stream profiles of $c_p u_p$, $c_p v_p$ and $u_p v_p$ are shown for the two different particle sizes at streamwise position $x = 250$ mm. The absolute values of the normalised correlation of particle velocity and concentration were smaller for the larger particle sizes. This occurs because of the increased inertia of the 90 μm particles relative to 55 μm. For both particles sizes, the correlation coefficient of the streamwise velocity and concentration was always higher than that of the cross-stream velocity and concentration on the high speed side. This may be due to the gravitational effects on particle dispersion, which can disperse particles in the cross-stream

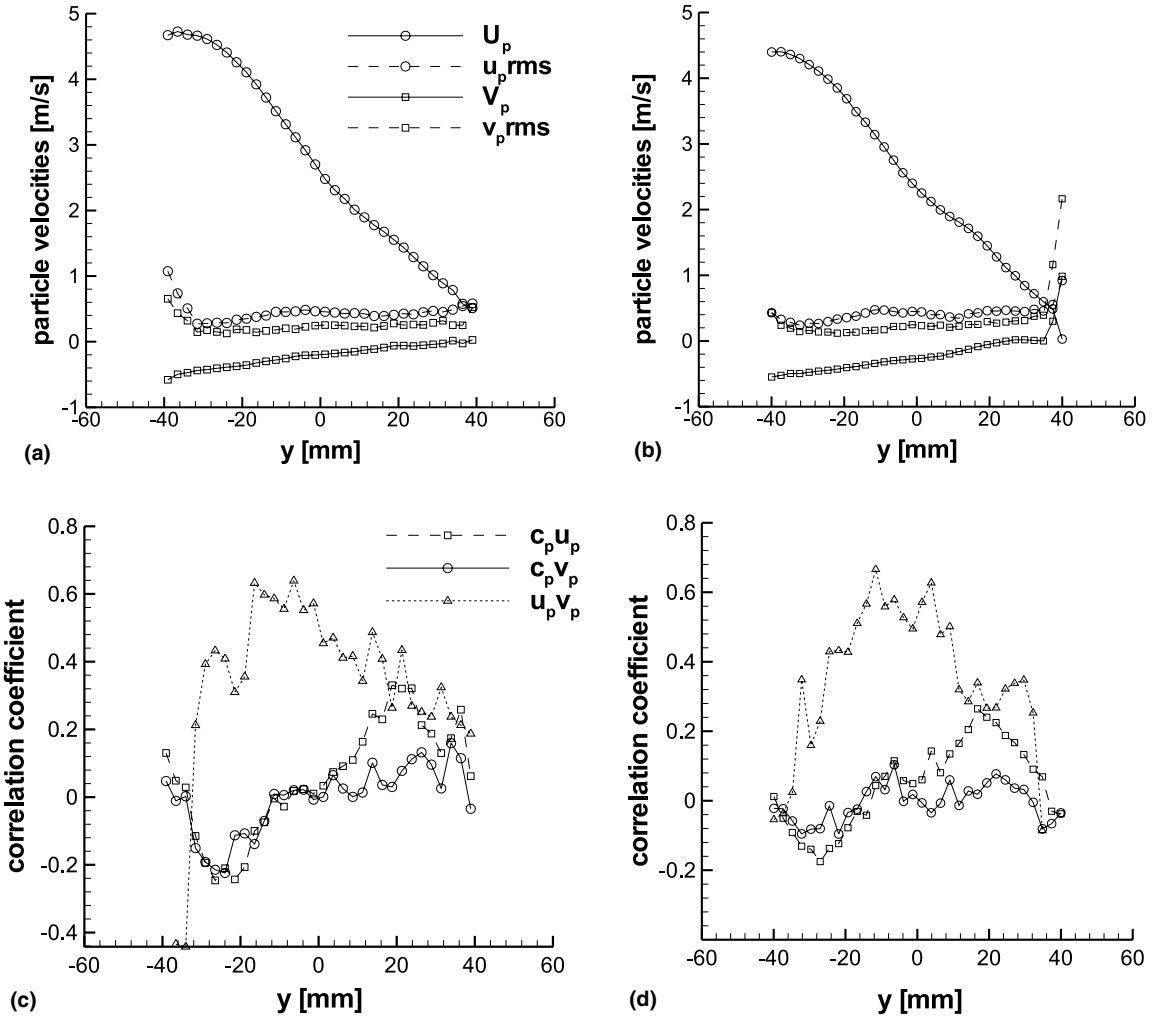

Fig. 11. Measured particle velocity profiles at streamwise position $x = 250$ mm for two different particle size classes: (a) 55 μm, (b) 90 μm. Cross-correlation coefficients of particle velocity and concentration fluctuations and cross-stream and streamwise velocity fluctuations for two size classes: (c) 55 μm and (d) 90 μm.

direction from the low speed to the high speed side, without any need for flow interaction to occur. The correlation between streamwise and cross-stream particle velocity components was around 0.6 for cross-stream positions, where most of the particles were located, and decreased for cross-stream positions away from the centre line. The measured cross-correlation terms of particle concentration and velocity are large and must be considered in any calculations of the modification of fluid flow turbulence (Eq. (1)). These are usually omitted as negligible, but current results suggest that these terms may be important. Work is in progress to quantify the importance of these terms on fluid flow turbulence modification.

The discrete vortex method was applied to calculate the fluid flow in the shear layer and consequently track particles through the flow, choosing particle relaxation time 50 ms, so that the

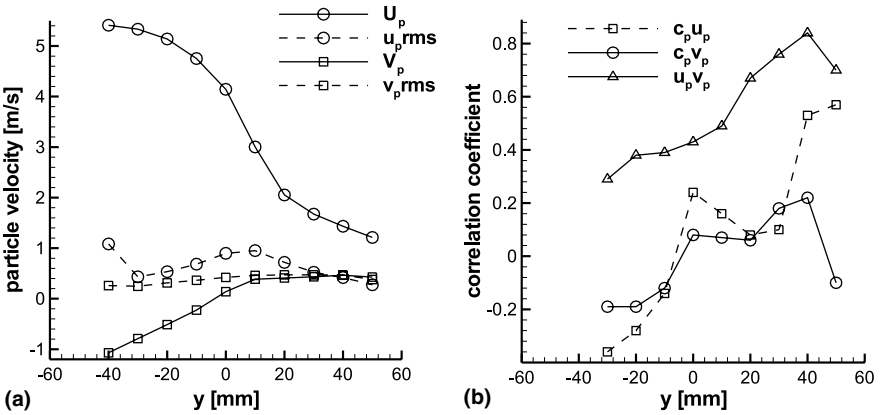

Fig. 12. Simulated particle velocity profiles and cross-correlation coefficients of particle velocity and concentration fluctuations and cross-stream and streamwise velocity fluctuations for streamwise position $x = 250$ mm for 90 μm particles.

Stokes number was around 1, as in the experiments for the 90 μm beads. Fig. 5 presented a resulting instantaneous particle dispersion pattern, while the flow direction was from left to right and particle clustering between the pairing vortices and centrifuging by the vortices can be observed.

Fig. 12(a) shows the simulated time-averaged particle velocity profiles, which follow the same trends as the measured profiles of Fig. 11(b) for 90 μm, e.g. the cross-stream velocity component is negative on the high speed side and positive on the low speed side of the shear layer. Hence, the discrete vortex model could predict the consequences of particle centrifuging on particle dispersion. The calculated rms of the cross-stream velocity of the particles is smaller than that for the streamwise velocity, which is the same trend as in the experiments. Therefore, particle rms velocities are mostly determined by centrifuging due to the large flow structures rather than response to the random small scale turbulent velocity fluctuations.

Fig. 12(b) shows the cross-correlation coefficients between concentration and velocity fluctuations $c_p u_p$ and $c_p v_p$, normalised by the corresponding rms of fluctuations, and the velocity cross-correlation coefficient $u_p v_p$ for streamwise location $x = 250$ mm and should be compared with the measurements of Fig. 11(d). It should be emphasised that the calculations did not include the gravitation effect. The symmetrical behaviour of the cross-correlation coefficients $c_p u_p$ and $c_p v_p$, observed in the experiments, around the centre of the shear layer was present only for $c_p v_p$ and not for $c_p u_p$, which was maximum at the low speed side of the shear layer. The cross-correlation coefficient of the velocities $u_p v_p$ was also not symmetrical in the calculations and higher than the experiments at the low speed side of the shear layer suggesting more deterministic particle trajectories. Considering that the particles at the low speed side are mainly arriving due to centrifuging the strong velocity correlation is expected. However, the experiments did not observe this effect. It is suggested that this is a consequence of the gravitational effect on particle dispersion, which has been important in the experiments and was not included in the calculations. Gravity dispersed particles away from the low speed side and reduced the correlation between the two particle velocity components and the concentration and streamwise velocity component. Current

work extends the calculations to include gravity and the findings are supportive of the above explanation. Therefore, the discrete vortex method can capture the physics of particle dispersion and calculate correctly the trends of the cross-correlation terms of both velocity components and concentration and the cross-correlation of the two velocity components. However, gravity effects are important and must be considered in the calculations. Additional parameters may influence the remaining discrepancies in absolute values at the high speed side of the shear layer and include the assumption of monosized 90 μm particles in the calculation, which could only respond to the large scale motion, while the size range used in the experiments was between 70 and 110 μm.

5. Conclusions

Measurements and calculations of mean and rms of fluctuations of particle velocities and concentration and cross-correlations coefficients of two particle velocity components and two particle velocity components and concentration fluctuations in a horizontal plane shear layer laden with glass beads with mean diameters 55 and 90 μm were presented. The particles were injected on the low speed side of the shear layer. The ranges of particle Stokes numbers were 0.2 to 0.6 and 0.6 to 1.4 for 55 and 90 μm respectively. The particle gravitational settling parameter, due to gravity acting normal to the main flow direction at the low speed side of the shear layer, was for the mean flow 0.2 and 0.5 and for the turbulent flow 0.5 and 1 for 55 and 90 μm respectively. Velocity measurements were obtained by particle image velocimetry (PIV) and instantaneous particle concentration by counting the number of particles in each interrogation cell of the PIV images. The effect of interrogation cell size on instantaneous particle concentration was assessed. Calculations of the fluid flow in the shear layer were performed based on the discrete vortex method, which satisfied the vorticity transport equation, and the discrete phase was calculated by Lagrangian particle tracking. The findings are summarised as follows:

(a) The intensity of spatially-resolved non-random concentration fluctuations varied between 0.6 and 0.9 of the local mean concentration at the edge of the shear layer, where particles dispersed only due to centrifuging by fluid flow large scale structures and between 0.15 and 0.35 in the central region of the shear layer, where particles are convected by the flow or arrive due to centrifuging from the fluid eddies and gravitational effects and, as a consequence, random contributions on particle concentration become more important. This finding suggests that the spatially averaged value of non-random particle concentration fluctuations does not represent correctly the particle flow characteristics.
(b) The rms of fluctuations of streamwise particle velocity was larger than that of the cross-stream velocity. The cross-correlation coefficient of fluctuations of particle concentration and streamwise particle velocity was 0.3, while that of the cross-stream particle velocity and concentration was smaller around 0.1. The cross-correlation coefficient of the fluctuations of the cross-stream and streamwise particle velocity components was around 0.6. The cross-correlation coefficients were symmetrical around the central region of the shear layer. Increased random flow motion, gravitational effects on particle dispersion and particle centrifuging determined the values at the central region and the gravitational influence may explain the lower value of the cross-correlation coefficient between particle cross-stream velocity and concentration

and the symmetry of the profiles. This finding was confirmed by appropriate quadrant analysis of the correlated measurements of velocity and concentration fluctuations.

(c) Discrete vortex calculations predicted fluid velocity frequency spectra with −5/3 decay, as measured in the experiments. The simulated results calculated qualitatively the experimental findings for particle mean and rms velocities. The calculated cross-correlation coefficients of particle concentration and velocities were not symmetrical and had higher values than the experiments at the low speed side of the shear layer. This is due to the effect of gravity on dispersion, which was not considered in the calculations, and confirmed the importance of gravity on particle dispersion.

(d) LIDAR systems for measurements of atmospheric turbulence must include an additional computation of the cross-correlation coefficient of scattered light intensity fluctuations (which is a measure of concentration fluctuations of scatterers) and measured velocity fluctuations, in order to assess potential bias in the velocity measurement due to preferential distribution of the scatterers. The size of the probe volume of such systems should be assessed in terms of the scale of the atmospheric turbulence or vortices of the wake of airplanes, in order to establish the influence of the averaging process over the probe volume on the detected signal.

References

Bernal, L.P., Roshko, A., 1986. Streamwise vortex structure in plane mixing layers. J. Fluid Mech. 170, 499–525.

Brown, G.L., Roshko, A., 1974. On density effects and large structures in turbulent mixing layers. J. Fluid Mech. 64, 775–816.

Chen, C.P., Wood, P.E., 1985. A turbulence closure model for dilute gas-particle flows. Can. J. Chem. Eng. 63, 349–360.

Chung, J.N., Troutt, T.R., 1988. Simulation of particle dispersion in an axisymmetric jet. J. Fluid Mech. 186, 199–222.

Crowe, C.T., Chung, J.N.C., Troutt, T.R., 1988. Particle mixing in free shear flows. Prog. Energy Combust. Sci. 14, 171–194.

Crowe, C.T., Troutt, T.R., Chung, J.N.C., 1996. Numerical models for two-phase turbulent flows. Ann. Rev. Fluid Mech. 28, 11–43.

Crowe, C., Sommerfeld, M., Tsuji, Y., 1997. Multiphase flows with droplets and particles. CRC Press.

Fessler, J.R., Kulick, J.D., Eaton, J.K., 1994. Preferential concentration of heavy particles in a turbulent channel flow. Phys. Fluids 6, 3742–3749.

Hardalupas, Y., Horender, S., 2000. Phase Doppler anemometer for instantaneous measurements of droplet concentration, 10th Int. Symp. Appl. Laser Tech. Fluid Mech., Lisbon.

Hardalupas, Y., Horender, S., 2001. Phase Doppler anemometer for measurements of deterministic spray unsteadiness, Part. Part. Syst. Charact 18, 205–215.

Huffaker, R.M., Hardesty, R.M., 1996. Remote sensing of atmospheric wind velocities using solid-state and CO_2 coherent laser systems. Proc. IEEE 84, 181–204.

Kiger, K.T., Lasheras, J.C., 1995. The effect of vortex pairing on particle dispersion and kinetic energy transfer in a two-phase turbulent shear layer. J. Fluid Mech. 302, 149–178.

Lázaro, B.J., Lasheras, J.C., 1992. Particle dispersion in the developing free shear layer. Part 1. Unforced flow. J. Fluid Mech. 235, 143–178.

Leonard, A., 1980. Vortex methods for flow simulation. J. Comp. Phys. 37, 289–335.

Ling, W., Chung, J.N., Troutt, T.R., Crowe, C.T., 1998. Direct numerical simulation of a three-dimensional temporal mixing layer with particle dispersion. J. Fluid Mech. 358, 61–85.

Longmire, E.K., Eaton, J.K., 1992. Structure of a particle-laden round jet. J. Fluid Mech. 236, 217–257.

Prevost, F., Boree, J., Nuclisch, H.J., Charnay, G., 1996. Measurements of fluid/particle correlated motion in the far field of an axisymmetric jet. Int. J. Multiphase Flow 22, 685–701.

Raffel, M., Willert, C., Kompenhans, J., 1998. Particle Image Velocimetry—A Practical Guide. Springer-Verlag, Berlin.
Sakakibara, J., Wicker, R.B., Eaton, J.K., 1996. Measurements of the particle-fluid velocity correlation and the extra dissipation in a round jet. Int. J. Multiphase Flow 22, 863–881.
Sarpkaya, T., 1989. Computational methods with vortices—The 1988 Freeman Scholar Lecture. J. Fluids Eng. 111, 5–52.
Sato, Y., 1995. Turbulence Structure and Modeling of Dispersed Two-Phase Flows, PhD Thesis, Keio University.
Shiels, D., 1998. Simulation of Controlled Bluff Body Flow with a Viscous Vortex Method, PhD Thesis, California Institute of Technology.
Soo, S.L., 1990. Comparison of formulation of multiphase flow, Keynote Lecture, Canadian Chemical Engineering Conference, Halifax, NS.
Tang, L., 1990. Simulation of Multiphase Free Shear Layers, PhD Thesis, Washington State University.
Tennekes, H., Lumley, J.L., 1972. A First Course in Turbulence. MIT Press. p. 67.
Van de Wall, R.E., Soo, S.L., 1994. Measurement of particle cloud density and velocity using laser devices. Powder Technol. 81, 269–278.
Yanta, W.J., Smith, R.A., 1978. Measurements of turbulence-transport quantities with a laser-Doppler velocimeter. AIAA paper no. 73-169. Presented at the 11th Aerospace Science meeting, Washington, DC.